63-4-1

QUARTERLY ENGINEERING REPORT NO. 4

INVESTIGATION OF ACTIVE DOPPLER VELOCITY SENSOR

1 MARCH 1963-31 MAY 1963

BR-2457
JUNE 1963

NAVIGATION AND GUIDANCE LABORATORY
AERONAUTICAL SYSTEMS DIVISION
AIR FORCE SYSTEMS COMMAND
UNITED STATES AIR FORCE
Wright-Patterson Air Force Base, Ohio

RAYTHEON COMPANY
SPACE AND INFORMATION SYSTEMS DIVISION

PREPARED UNDER CONTRACT No. AF33(657)-9241

INVESTIGATION OF ACTIVE DOPPLER VELOCITY SENSOR

RAYTHEON COMPANY
SPACE AND INFORMATION SYSTEMS DIVISION
BEDFORD, MASSACHUSETTS

QUARTERLY ENGINEERING REPORT NO. 4
1 MARCH 1963-31 MAY 1963
CONTRACT No. AF33(657)-9241

BR-2457 JUNE 1963

NAVIGATION AND GUIDANCE LABORATORY
AERONAUTICAL SYSTEMS DIVISION
AIR FORCE SYSTEMS COMMAND
UNITED STATES AIR FORCE
Wright-Patterson Air Force Base, Ohio

ABSTRACT

This material is submitted as Quarterly Report No. 4 on the Active Doppler Velocity Sensor (ADVS) program under Contract AF33(657)-9241 for the Navigation and Guidance Laboratory, Aeronautical Systems Division (ASD) and represents the results, to date, of a study program directed toward the advancement of the state-of-the-art of Doppler navigation radar techniques to meet the high speed, high altitude requirements of an aerospace vehicle.

Under the contract, demonstration of satisfactory completion of the program will consist of sound theoretical proofs that the system techniques evolved are feasible, and working breadboards of critical system areas with necessary instrumentation.

During this reporting period, flight testing of the manual spectral compression system began, with bandwidth compression ratios of the order of 10 to 1 being achieved. The preliminary development of the Computer and Control unit was completed, and fabrication of the flyable model was essentially completed. The Computer and Control unit was designed to evaluate the two types of velocity determination: modulation slope dependent; and modulation slope independent.

This report is, then, a record of Raytheon's progress toward the specified contract objectives.

TABLE OF CONTENTS

LIST OF ILLUSTRATIONS

1. PURPOSE

1.1 Aims of the Investigation

The Navigation and Guidance Laboratory at ASD has set forth the statement of the general problem.

1.1.1 Statement of the Problem

To meet future Air Force requirements in the space vehicle guidance area, new highly advanced navigation sensors must be developed. The Active Doppler Velocity Sensor (ADVS) will give the velocity of a space vehicle with respect to a planetary surface by detecting the Doppler frequency shift between the transmitted signal and the return signal reflected from the planetary surface. Potential mission applications of this Doppler velocity sensor are:

1) determine velocity and position (integration of velocity by a computer on the vehicle) of an aerospace vehicle and allow it to locate a target;
2) give accurate velocity information to a descending aerospace vehicle to permit proper deceleration and landing.

The Active Doppler Velocity Sensor shall be an accurate, fully automatic, self-contained equipment capable of operation at extreme altitudes over all types of terrain, including water surfaces. In order to attain the large increase in operational capability over present doppler radars, significant state-of-the-art advances in techniques will be required in the receiving and signal processing networks.

1.1.2 Objective

The objective of this program is the investigation (including the breadboarding of experimental assemblies) of improved techniques in certain critical portions of doppler velocity sensors. Improvements in these critical areas will permit the Active Doppler Velocity Sensor to operate over an

altitude range of 100 nautical miles over all types of terrain, including water surfaces (Aerospace vehicle applications). The sensor should be capable of operating over a velocity range of up to 25,000 feet per second, and give a velocity in vehicle coordinates with an accuracy of plus or minus 10 feet per second over this range, and plus or minus 3 feet per second over the range of 0 to 1,000 feet per second. The primary end result of this work is the development of a spectral compression technique which aims to reduce transmitter power requirements, eliminate terrain bias error, and reduce fluctuation error. The development of this advanced technique will constitute a significant improvement over present doppler radar techniques, and will contribute directly in reaching the high altitude-range goal of the proposed Active Doppler Velocity Sensor.

1.2 Division of Effort

During this reporting period, flight testing of the manual spectral compression system was performed. Development and fabrication of the flyable model of the Computer and Control unit was completed.

Three customer-contractor meetings were held during this reporting period. On March 21 and 22, 1963, Mr. D. Guidice of ASD visited Raytheon to review technical progress with the ADVS Project Team. Mr. Guidice also visited Raytheon on April 16, 1963, to review the results of the first spectral compression flight. On May 28, 1963, Messrs. A. Chabot, D. Delgrego and J. Rand of Raytheon visited Messrs. D. Guidice and G. Pasek of ASD to review the flight test results, and to flight demonstrate the manual spectral compression system in Raytheon's B-26 Aircraft.

1.2.1 Spectral Compression

Flight testing of the manual spectral compression system was completed during this reporting period. Development and fabrication of the flyable model of the Computer and Control unit was essentially completed. As the reporting period drew to a close, ground checkout of the unit was in progress.

1.2.1.1 Wide Deviation FM Generator

Flight evaluation of this system showed that any excess amount of acoustic noise would cause FM noise. Attention was directed toward tube selection and acoustic shielding. Closed loop stability of the VCO was also improved. Measurements were also made of the linearity of the diode-rate counter that stabilizes the VCO.

1.2.1.2 Computer and Control Unit

With development and fabrication of the flyable model having been completed, attention has been directed toward ground checkout of the Computer and Control Unit.

1.2.1.3 Flight Testing

Flight testing of the manual spectral compression system has been performed at ground speeds between 170 and 300 kts and altitudes up to 10,000 feet above terrain. Rough terrain, flat land, water return, and drift angle effects have been investigated. Special attention has been paid toward reducing the frequency fluctuations in the tape recording equipment so that the narrow bandwidths achieved in flight may be truly viewed on the ground.

1.2.1.4 Analysis

The optimum form of the bandwidth sensor for automatic slope control was determined.

2. DISCUSSION

The following sections contain a general discussion of the spectral compression system that is being flight tested, along with a detailed review of the development activity to date, on the components of the system.

2.1 Experimental System

Only two changes have been made that would affect the system block diagram (Figure 2-1 of Reference 1). The 10 kc Rayspan analyzer has been replaced with a 3 kc unit to improve in-flight bandwidth resolving capability. Resolution in the first unit was limited to 75 cps, whereas the 3 kc unit can resolve down to 25 cps. A doppler mixer has been added so that the high beat frequencies of 20 - 30 kc may be heterodyned to 2 kc before recording, to reduce tape flutter and wow effects. A description of this doppler mixer is contained in Section 2.2.

Figures 2-1 and 2-2 show the system and instrumentation racks installed in the B-26 aircraft. Figure 2-3 shows the power supply rack, the recorder, and the drift sight also installed in the B-26 aircraft.

2.1.1 Master FM Oscillator Unit

2.1.1.1 Voltage Controlled Oscillator (VCO) Loop

Since the linearity of the frequency sweep is of primary importance to good spectral compression, an attempt has been made to get more precise measurements of the VCO linearity. One has shown in earlier reports that the transmitter frequency is controlled by an AFC loop in which a biased, diode-rate-counter is used as the frequency controlling element. The open loop gain of the AFC loop is sufficiently high (in excess of 60 db) that the transmitted waveform will essentially be the inverse of the diode-rate-counter characteristics. Measurements of the counter should, therefore, be a measure of transmitter linearity. The test setup of Figure 2-4 was used to make static measurements of counter linearity. One of the problems of trying to measure linearity by static measurements is that the counter has a small amount of slow drift.

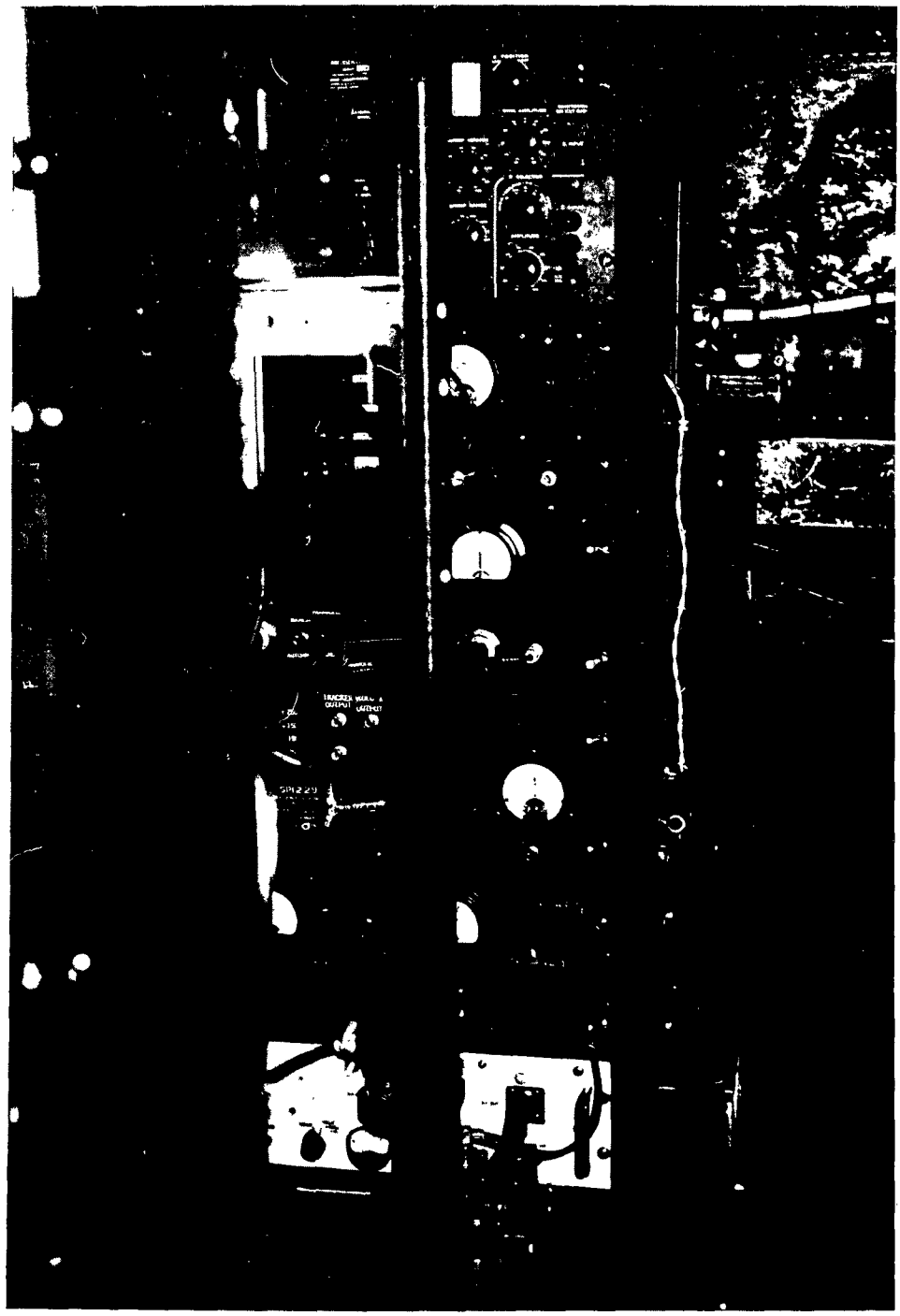

Figure 2-1 - System Rack

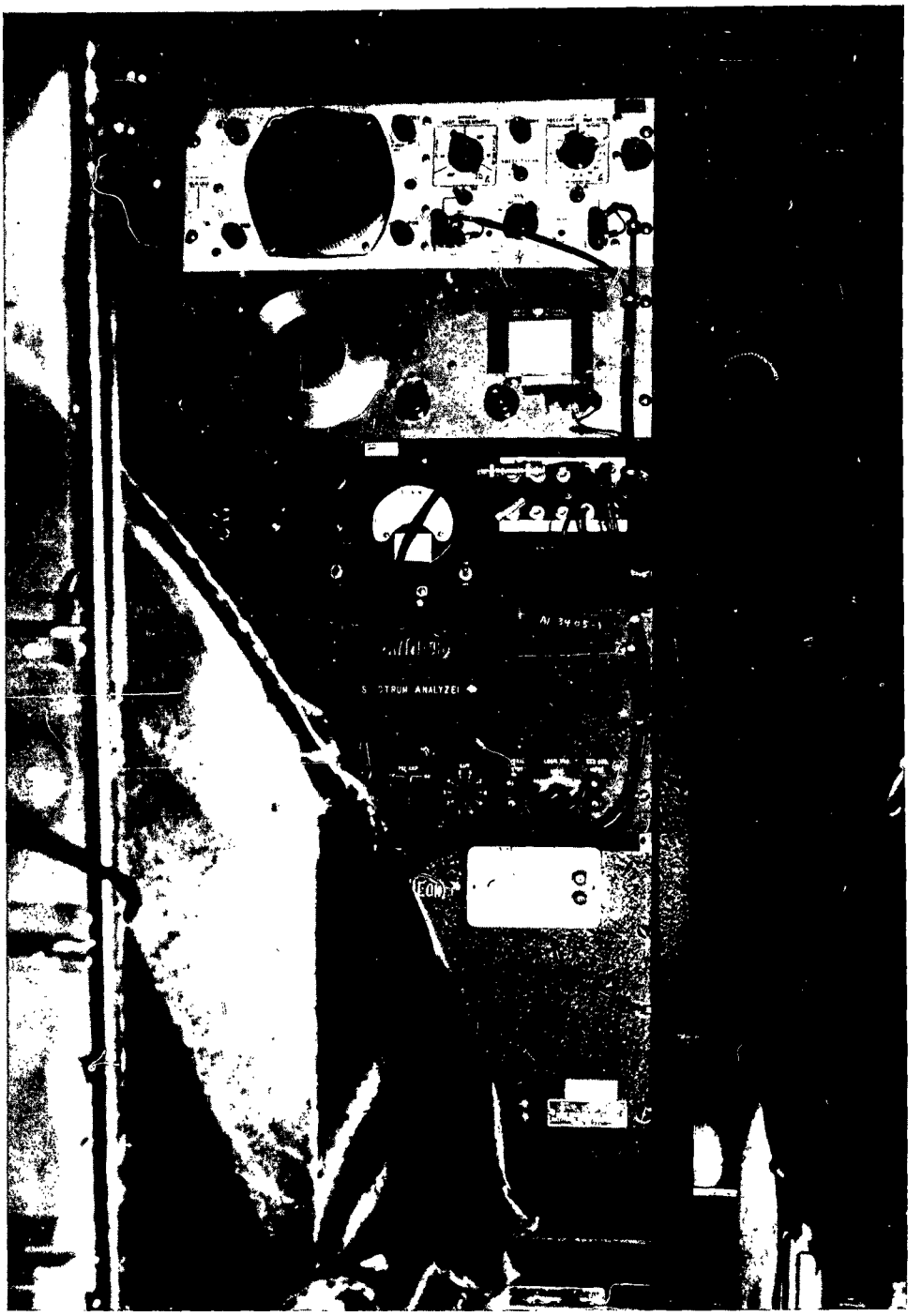

Figure 2-2 - Instrumentation Rack

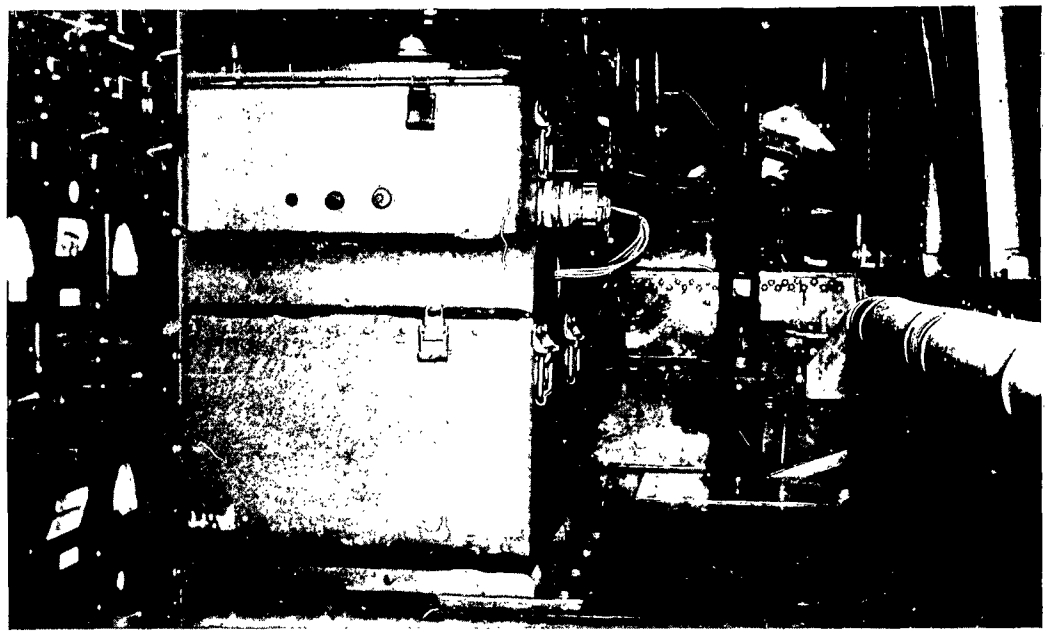

Figure 2-3 - Auxiliary Aircraft Equipment

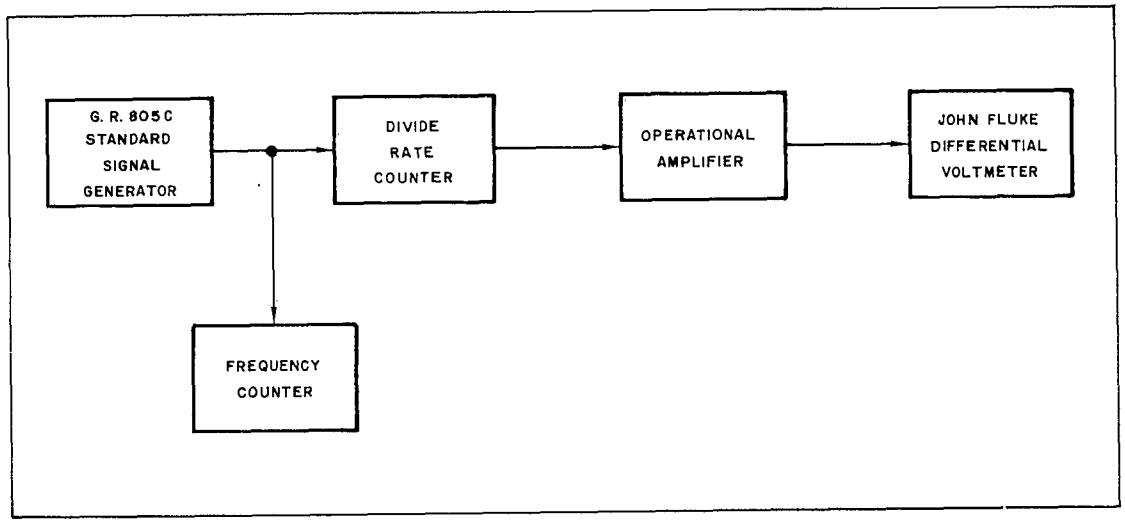

Figure 2-4 - Static Measurement of Diode-Rate-Counter Linearity, Block Diagram

Although this normally amounts to but a few hundred cycles, and does not affect the doppler signal, it does complicate any precise linearity measurements. To get a measure of any long-term drift over the measuring interval, data was taken: first, starting at a high frequency and working to a low frequency (Data No. 1); and then starting at a low frequency and working to a high frequency (Data No. 2). In each case, a straight line was fitted to the data. Any change in slope between the two sets of data was assumed to be an indication of drift. The method used to fit a straight line to the data is the method of least squares. A formula of the form of Equation 2-1 is desired:

$$f = a_1 + a_2 e \tag{2-1}$$

where,

f = frequency
e = voltage

The coefficients a_1 and a_2 (slope) may be solved by using Equations (2-2) and (2-3):

$$n\, a_1 + \left(\sum_{i=1}^{n} e_i\right) a_2 = \sum_{i=1}^{n} f_i \tag{2-2}$$

$$\left(\sum_{i=1}^{n} e_i\right) a_1 + \left(\sum_{i=1}^{n} e_i^2\right) a_2 = \sum_{i=1}^{n} e_i f_i \tag{2-3}$$

Solving for the coefficients a_1 and a_2 for the measured data yields the following two equations:

$$f = -99.0 + 16,555.6\, e \tag{2-4}$$
$$f = -109.4 + 16,562.8\, e \tag{2-5}$$

Equation (2-4) was obtained from Data No. 1 and Equation (2-5) from Data No. 2. In each case, the lowest frequency and lowest voltage were considered to be zero.

The difference frequency was taken between the theoretical and measured data and plotted in Figure 2-5, according to the following:

$$\Delta f_i = f - f_i. \tag{2-6}$$

As can be seen from the curves of Figure 2-5, both sets of data indicate a predominant second order nonlinearity. To get an indication of this distortion, a formula of the following form is desired:

$$f = a_1 + a_2 e + a_3 e^2. \tag{2-7}$$

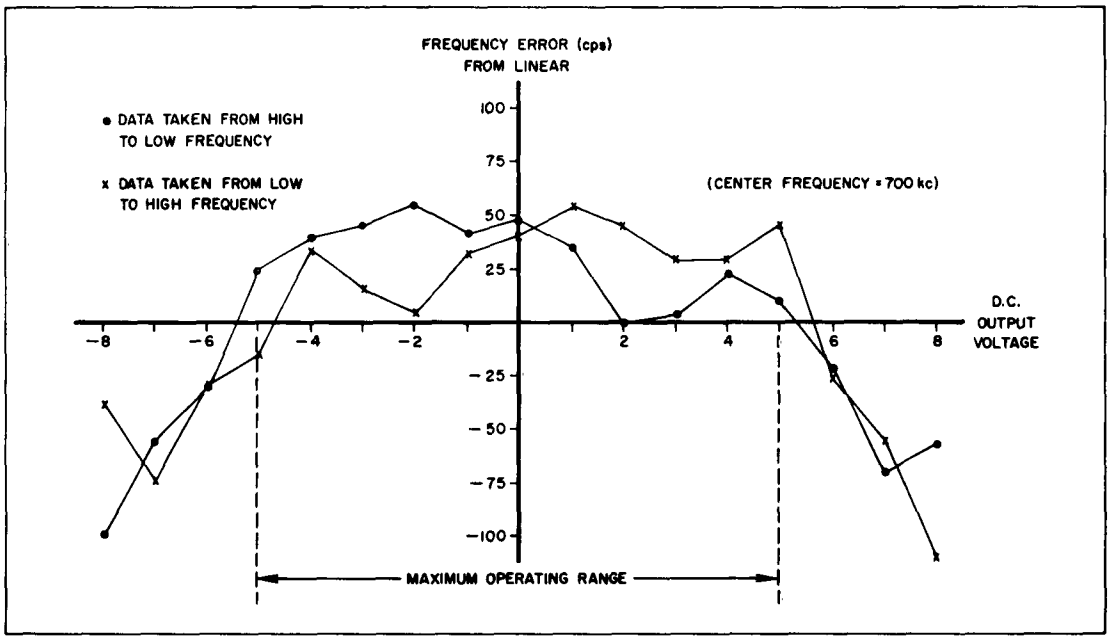

Figure 2-5 - Diode-Rate-Counter Error for Linear Function

The distortion is again found by using the method of least squares and solving the following set of equations:

$$n\,a_1 + \left(\sum_{i=1}^{n} e_i\right) a_2 + \left(\sum_{i=1}^{n} e_i^2\right) a_3 = \sum_{i=1}^{n} f_i \qquad (2\text{-}8)$$

$$\left(\sum_{i=1}^{n} e_i\right) a_1 + \left(\sum_{i=1}^{n} e_i^2\right) a_2 + \left(\sum_{i=1}^{n} e_i^3\right) a_3 = \sum_{i=1}^{n} e_i f_i \qquad (2\text{-}9)$$

$$\left(\sum_{i=1}^{n} e_i^2\right) a_1 + \left(\sum_{i=1}^{n} e_i^3\right) a_2 + \left(\sum_{i=1}^{n} e_i^4\right) a_3 = \sum_{i=1}^{n} e_i^2 f_i \qquad (2\text{-}10)$$

Since both curves plotted in Figure 2-5 have similar shapes, only the data taken from low to high frequency was fitted with the second order correction. For that set of data, Equation (2-11) was obtained:

$$f = -126.9 + 16,554.3\,e + 0.8029\,e^2. \qquad (2\text{-}11)$$

In this case, only data from +5 to -5 volts was used as this is the maximum swing of the VCO. Again, the difference frequency was taken between the theoretical formula (Equation 2-11) and the measured data. The result is plotted in Figure 2-6.

The maximum deviation error from a straight line may be computed using Equation (2-12):

$$\epsilon = \frac{a_3\,e_m}{4\,a_2} \qquad (2\text{-}12)$$

where e_m is the maximum voltage (+10 volts).
Substituting the values from Equation (2-11) into Equation (2-12):

$$\epsilon = \frac{(0.8029)\,(10)}{(4)(16,554.3)} = 1.22 \times 10^{-4} \text{ or } 0.0122\% \qquad (2\text{-}13)$$

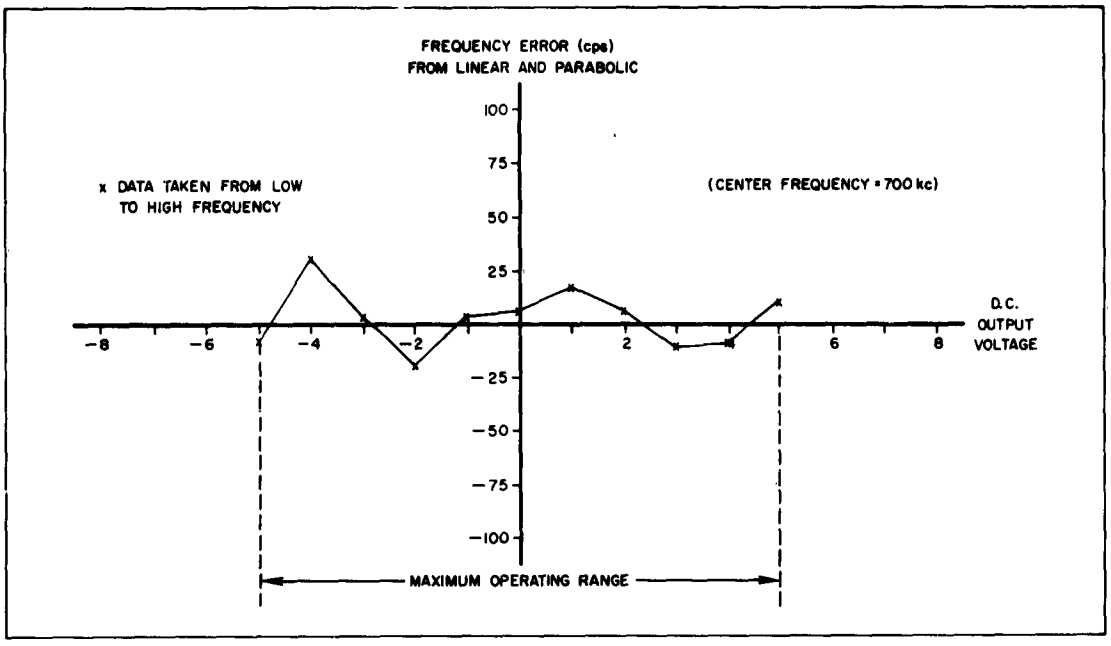

Figure 2-6 - Diode-Rate-Counter Error for Linear and Parabolic Function

As stated earlier, data was taken in both directions to try to determine the effects of drift. The change in slope may be determined by Equations (2-4) and (2-5) as:

$$\Delta a_2 = 16,542.8(16) - 16,555.6(16) = 115.2 \text{ cycles} \qquad (2\text{-}14)$$

This drift is in a direction so as to increase any measured nonlinearity.

2.1.1.2 UHF and RF Harmonic Multipliers

Since the last report (Reference 1), a new microwave multiplier has been installed in the system. The new multiplier has improved response over the 200 mc bandwidth. A photograph of the transmitter bandpass (saturated TWT) is shown in Figure 2-7. The microwave power output is in excess of 7 watts. Markers are provided in the photo by passing the swept signal through a tuneable cavity before detecting.

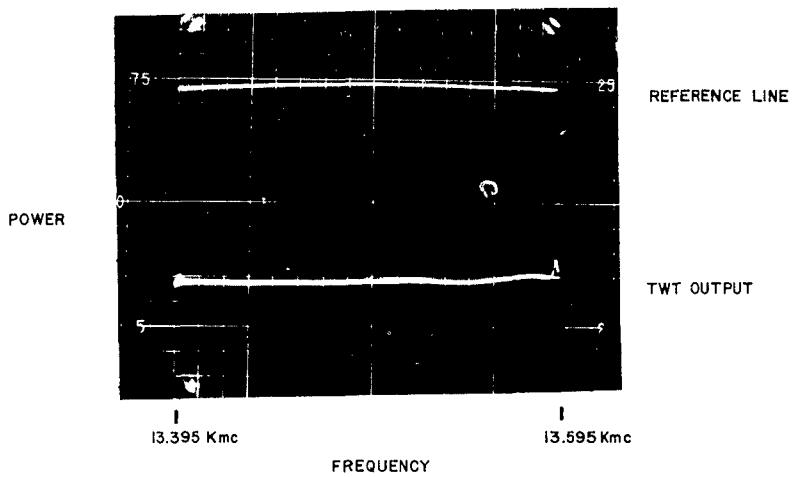

Figure 2-7 - Transmitter Bandpass

2.1.1.3 VCO FM Noise

In Reference 1, the technique for measuring transmitter FM noise using a microwave pound discriminator was discussed. During this reporting period, one determined that comparable measurements could be made using the built-in microwave cavity used for measuring transmitter frequency. This method of FM measurement uses the tuned cavity as a slope detector and normally suffers from the disadvantage that it is sensitive to AM as well as FM. However, since the TWT amplifier is operating in saturation, AM components are eliminated. In operation, the detector is calibrated by feeding 10 millivolts of 1 kc signal into the VCO. The pushing figure of the loop is:

$$S = \frac{10^8 \text{ (cps peak)}}{3.53\ V_{rms}} \qquad (2\text{-}15)$$

A signal of 10 millivolts produces 283 kc of peak deviation, and an output from the cavity of 35 millivolts (this figure will vary depending on the amount of power into the cavity, and is checked each time FM is measured).

The received modulation index of a coherent, frequency-modulated doppler system may be determined from Equation (2-16) below:

$$\delta = 2\,\Delta f\,(6.38 \times 10^{-9}\,\frac{h}{\sin\gamma})\left[\frac{\sin(6.38\times10^{-9}\,\frac{h}{\sin\gamma}\,f_m}{6.38\times10^{-9}\,\frac{h}{\sin\gamma}\,f_m}\right] \qquad (2\text{-}16)$$

where: Δf = peak frequency deviation (cps)
h = aircraft altitude (feet)
γ = antenna depression angle (70°)
f_m = modulating frequency (cps)

The bracketed part of Equation (2-16) has the form $\frac{\sin x}{x}$, and approaches unity as x approaches zero. This form may, therefore, be considered unity for altitudes of less than 8,000 feet and modulating frequencies of less than 10 kc. Under these conditions:

$$\delta \approx 1.365 \times 10^{-8}\,\Delta f\,h \qquad (2\text{-}17)$$

If at an altitude of 8,000 feet, one desired to keep the carrier loss less than 3 db ($\delta = 1.1$), the allowable FM deviation may be calculated to be:

$$\Delta f = \frac{\delta}{1.365 \times 10^{-8}\,h} = \frac{1.1}{(1.365\times10^{-8})(8 \times 10^{3})} = 10.1 \text{ kc} \qquad (2\text{-}18)$$

Although many precautions were initially taken to shock mount the racks and operational amplifiers in the transmitter, initial FM measurements with engine run-up showed the transmitter FM to be about 24 kc (peak). The major source

of FM was traced to 8 kc and 4 kc components caused by acoustic sensitivity of the nuvistor tubes used in the operational amplifier of the feedback loop. By picking low microphonic tubes and acoustic shielding of the nuvistors, the FM noise was reduced to 7.4 kc (peak). This amount of FM has allowed successful flights to altitudes of 8,000 feet and more.

2.1.2 Computer and Control Unit

The Computer and Control unit (Figure 2-8) has been completely fabricated and consists of an automatic slope control loop, and a doppler frequency computer. The simplest machine equation for the computation of doppler frequency was determined, in Reference 1, to be:

$$f_{D_i} = \frac{f'_{B_i}(1 - \delta) - f''_{B_i}(1 + \delta)}{2\delta} \qquad (2\text{-}19)$$

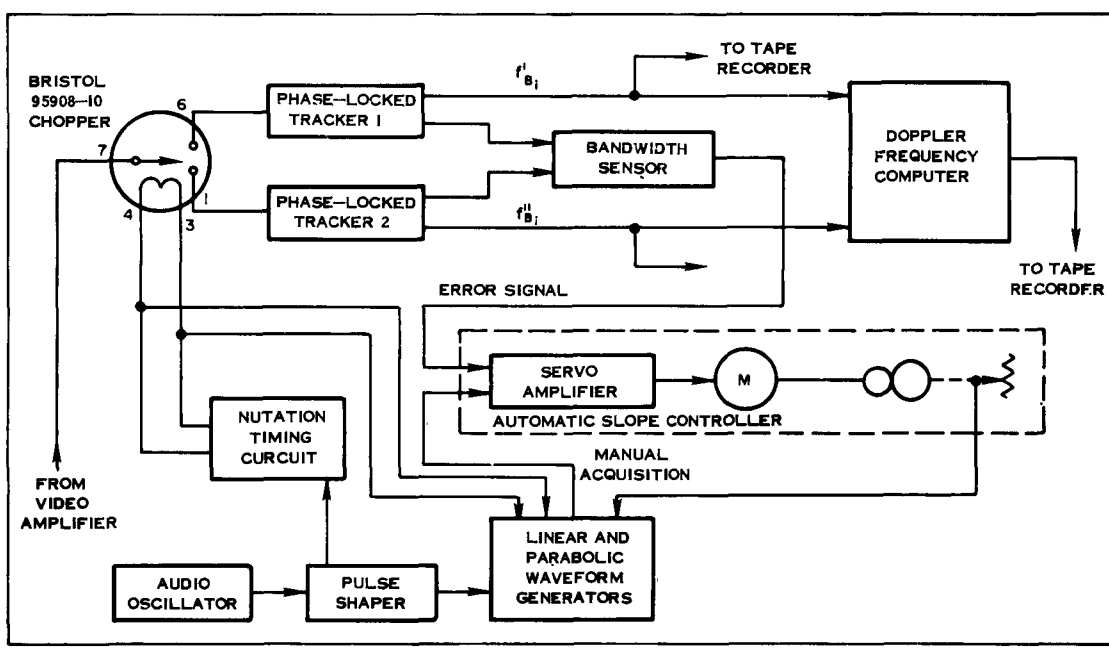

Figure 2-8 - Computer and Control Unit, Block Diagram

where

f_{D_i} = Doppler frequency in i th channel

f'_{B_i} = Beat frequency for high nutation

f''_{B_i} = Beat frequency for low nutation

δ = Modulation slope increment

For $\delta = 0.1$, the doppler frequency (after some manipulation) becomes:

$$f_{D_i} = 2.75 \left(2 \times 0.818182\, f'_{B_i} - 2\, f''_{B_i}\right) \tag{2-20}$$

and this is the machine equation recommended in Reference 1. However, since that time, an even simpler equation (for machine computation) was found to exist, which corresponds to a δ of 0.1034483. For this modulation slope increment, the doppler frequency reduces to:

$$f_{D_i} = 5.333 \left(\frac{4.333}{5.333}\, f'_{B_i} - f''_{B_i}\right) \tag{2-21}$$

or

$$f_{D_i} = \frac{5.333}{2} \left[2 \times 0.81250\, f'_{B_i} - 2\, f''_{B_i}\right] \tag{2-22}$$

Equation (2-22) is simpler to instrument than Equation (2-20), and has been chosen for the system. This new selection of $\delta = 0.1034483$ required that the summing resistor in the voltage waveform generator be changed to permit the somewhat higher modulation slope increment. Figures 2-9, 2-10, and 2-11 are photographs of the Computer and Control Unit in three (3) different views.

Figure 2-9 - Computer and Control Unit, Front and Top View

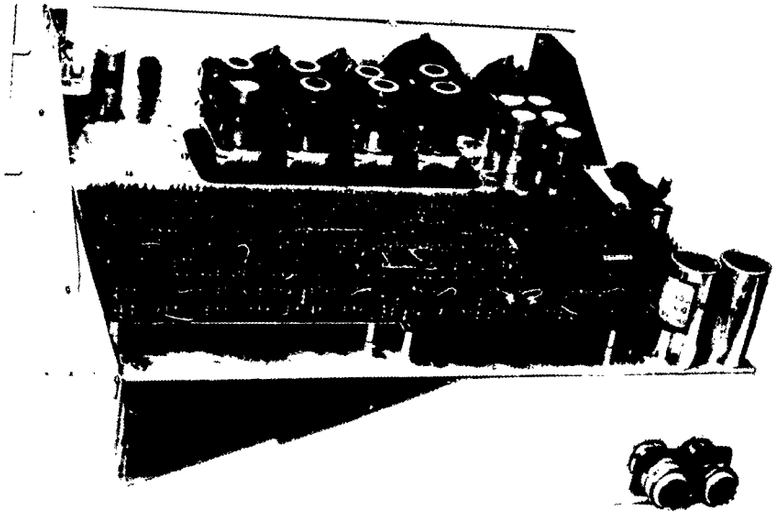

Figure 2-10 - Computer and Control Unit, Back and Top View

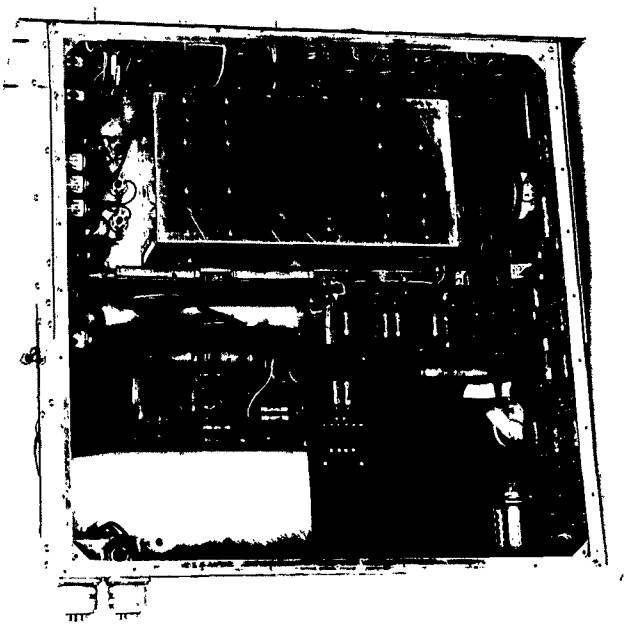

Figure 2-11 - Computer and Control Unit, Bottom View

2.1.2.1 Automatic Slope Control Loop

The elements of the Automatic Slope Control Loop are the same as those described in Reference 1 and shown in Figure 2-8 and are as follows:

1) Nutating timing and switching,
2) Two (2) phase-locked frèquency trackers, including optimum filtering circuits,
3) Two (2) bandwidth sensors,
4) Error amplifier and control circuit (Automatic slope controller),
5) Voltage waveform generator.

During this reporting period, considerable effort was directed toward constructing, testing, and improving those circuits described in Reference 1. All of the flyable breadboards have been tested, and found to operate satisfactorily. The following subparagraphs describe, in a more detailed manner, the elements of the Automatic Slope Control Loop.

Nutation Timing Circuit

The nutation timing circuit will provide the switching for the automatic slope control loop. Design requirements of the nutation timing circuit were described in Reference 1. A flyable breadboard model of the nutation timing circuit has been built and tested, and a schematic of this unit is shown in Figure 2-12.

The basic PRF from the Voltage Waveform Generator is divided by either eight (8) or sixteen (16). This square wave output passes through a transistorized Darlington amplifier, which then feeds two (2) transistor power amplifiers. The power amplifiers provide two (2) states of operation corresponding to the two (2) extremities of the input square wave. Each of these states of operation drives the chopper coils and contacts by approximately equal amounts to either side of neutral, thus providing the desired nutation switching.

The nutation timing circuit was tested with an input of 16 cps, which approximates flight conditions. The design requirement calls for each contact to be actuated by equal amounts, to an accuracy of 0.1%. Utilizing the divide by sixteen (16) output, time interval measurements made on the resulting

waveform verified that the duration of each half cycle was approximately 500 milliseconds, with a variation of approximately 500 microseconds. Therefore, this nutation timing circuit should be satisfactory.

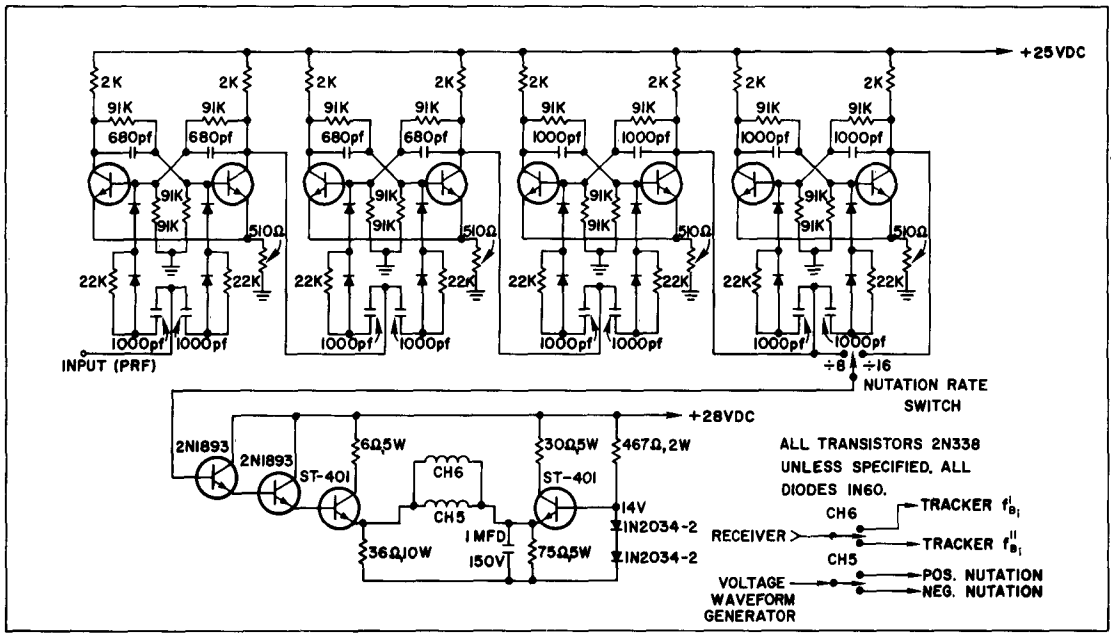

Figure 2-12 - Nutation Timing Circuit, Schematic

Phase-Locked Tracker

During this reporting period the design of the tracker was finalized and two (2) trackers, to be utilized in the automatic slope control loop, have been fabricated as part of the Computer and Control unit. The latest schematic of the phase-locked tracker is included in Figure 2-13.

The tracker is basically similar to the original design. However, certain changes and improvements have been incorporated. Most important of these is improvement of the acquisition circuit by installing a separate

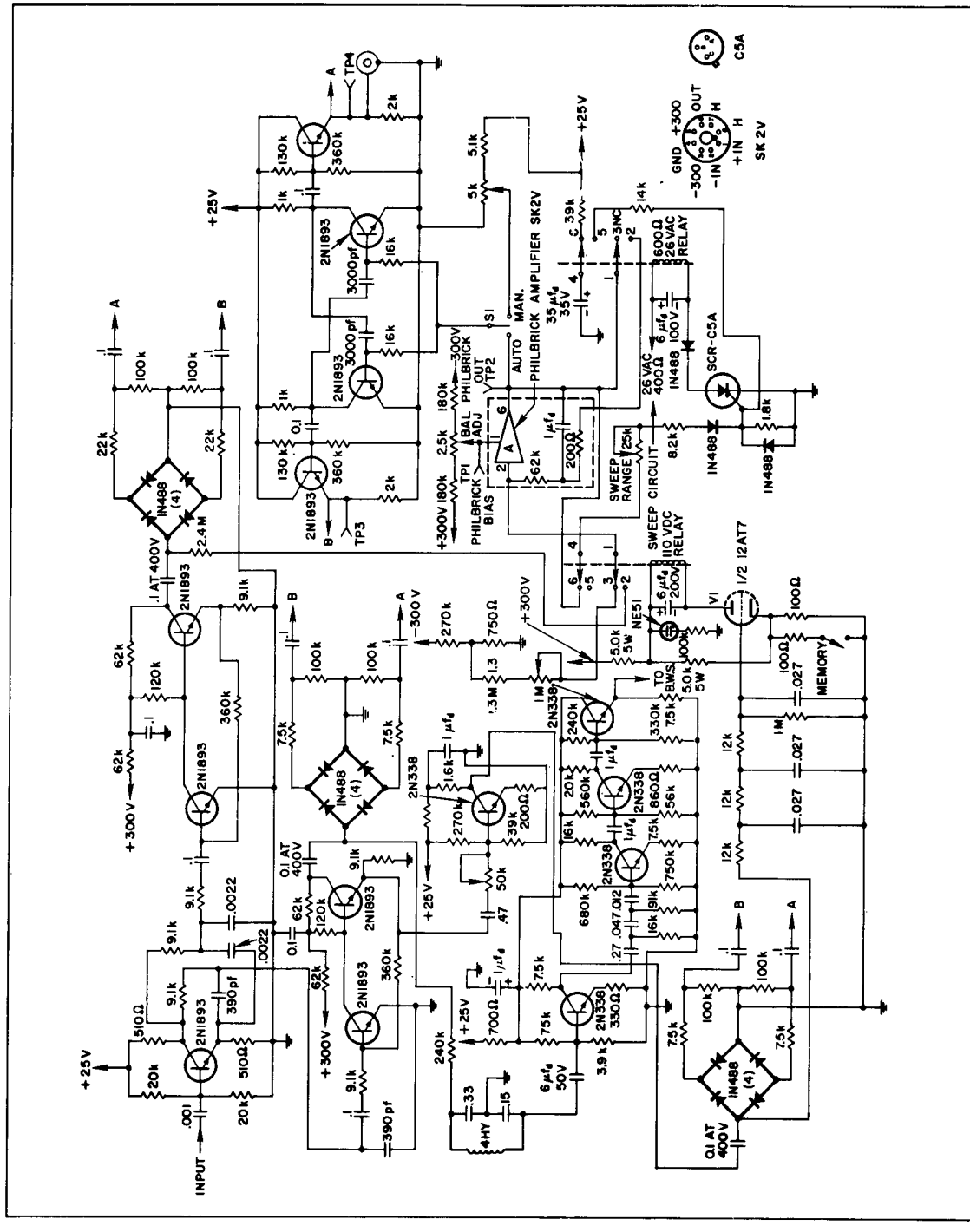

Figure 2-13 - Phase Locked Tracker, Schematic

phase comparison network to drive a tube and relay circuit. Also the base band spectrum output (bandwidth sensor input) has been separated from the acquisition circuit, and optimum filtering, as described in Section 2.3 and Appendix A, has been designed and incorporated.

Three phase comparison networks are now included in the tracker. One of these (as before) is in the closed loop which keeps the local oscillator phase-locked to the input spectrum. A second phase comparison circuit translates the beat frequency spectrum to base band for use as the input to the bandwidth sensor circuits. The third phase comparison circuit provides a dc output to drive the acquisition circuit. This latter circuit incorporates a memory feature that will enable the tracker, once locked, to remain locked, and thus be relatively insensitive to short periods of absence of the input spectrum.

The tracker has been tested in the laboratory using tape recordings taken during ADVS flights. These tests, although not complete, have been very satisfactory since they demonstrated that the tracker can search for, acquire, and track the beat frequency spectrum, while supplying a base-band output spectrum to the bandwidth sensor circuits.

At the present time no serious problems are anticipated with the phase-locked tracker and associated circuitry. During the next period, major effort will be applied toward installation and testing of the flyable models of the tracker.

Optimum Filter - Bandwidth Sensor

The optimum filter for the bandwidth sensor circuits has been chosen on the basis of the analyses presented in Section 2.3 and Appendix A, and the practical considerations may now be discussed. Mathematically, the optimum filter is given as:

$$D_{opt}(f) = k \frac{f^{2p}}{\left(B^{2p}\left(1+\frac{S}{N}\right)+f^{2p}\right)^2} \qquad (2\text{-}23)$$

where p is the order of the Butterworth signal spectrum which most closely fits the over-all antenna transmit-receive pattern.

Knowledge of the antenna patterns indicates a composite return spectrum that slopes at a rate somewhat greater than 12 db/octave. To simulate this, a p equal to 2 (second order Butterworth) appears most appropriate.

Referring to paragraph 2.3.1.3 one concluded that, for a fixed design employed for a range of spectra of differing widths, the filter characteristic should be somewhat less sharp in rise and fall than theory indicates as optimum for a fixed bandwidth. Based on this knowledge, one concluded that the optimum filter should have a rise and fall of at least 12 db/octave. Also, one concluded that the filter's rise slope was more critical than its fall slope in the presence of high signal-to-noise ratios and, therefore, a sharper than theoretical roll-off should not appreciably affect the bandwidth sensor output.

The optimum filter presently incorporated has a rise slope of approximately 12 db/octave while the fall slope is greater than 12 db/octave but less than 18 db/octave. Corner frequencies are located approximately where dictated by the theory of Section 2.3 and Appendix A.

The optimum filter was designed as part of the phase-locked tracker unit. As before, the tracker output will feed the bandwidth sensing circuits.

Response of the optimum filter has been observed in the laboratory using a white noise source feeding a variable, low-pass, SKL filter to simulate a baseband spectrum. By varying the SKL filter bandwidth while measuring the dc output of the bandwidth sensor channels, response curves were obtained. Typical curves obtained with and without optimum filtering are shown in Figure 2-14. Scale factors thus far observed are approximately 1.3 mv/cps without optimum filtering versus approximately 7 mv/cps with optimum filtering. Two important results of optimum filtering (which were anticipated) appear to be realizable; namely, increased scale factor and a reduction of output fluctuations.

Figure 2-15 is the latest schematic of the bandwidth sensor. Discussion of this circuit is included in Reference 1. Minor improvements for stability have been made and, in addition, a bandwidth sensor meter with provisions for calibration has been incorporated. Calibration consists of feeding in a known bandwidth (for example, 50 cps) from the white noise source and SKL filter, and adjusting the potentiometer for a meter reading twice this value (100 cps). This accounts for fold over of the spectrum occurring at the tracker output. The time constant of the meter is approximately equal to the time

constant of the bandwidth sensor circuit. The above design appears to be satisfactory, and further testing will be conducted during the next period to verify the design.

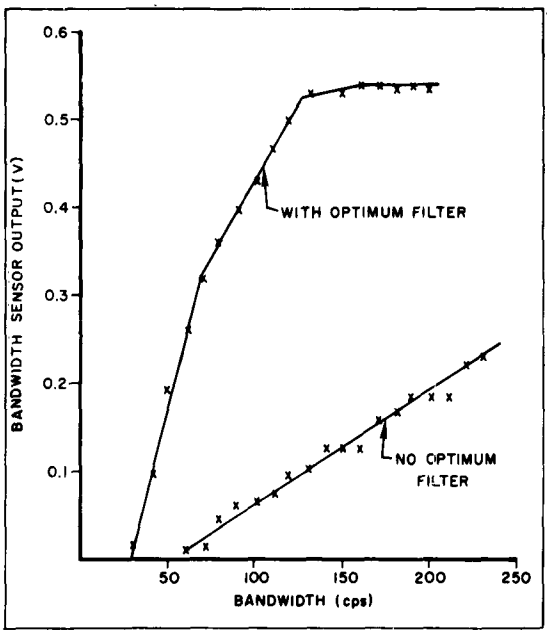

Figure 2-14 - Bandwidth Sensor Response vs Bandwidth Input

Automatic Slope Controller

The automatic slope controller, which will be the error signal amplifier and control circuit of the Automatic Slope Control Loop, was described in Reference 1. During this reporting period, the flyable model of the automatic slope controller has been under construction and will be tested when completed, along with the other elements of the Automatic Slope Control Loop.

The automatic slope control simulation plan, which was to have demonstrated closed loop performance of the Automatic Slope Controller, was also described in Reference 1. This test was not performed since it was determined that the Bandwidth Simulator, which was to have simulated beat frequency

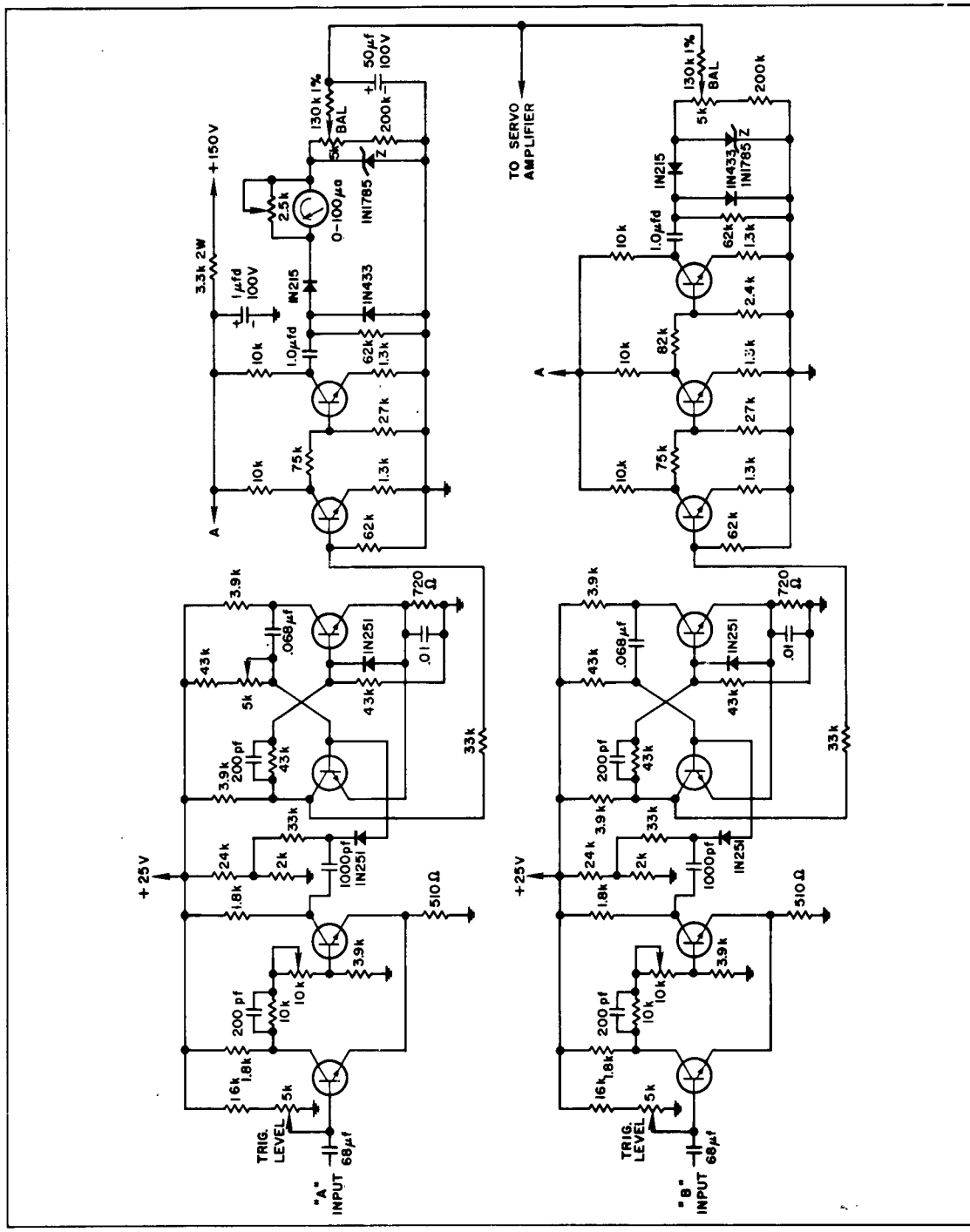

Figure 2-15 - Bandwidth Sensor, Schematic

spectra, was not a suitable signal source. This was because the slope of the spectrum was only 6 db per octave (single tuned circuit) whereas it was later determined that slopes equal to or greater than 12 db per octave are required to simulate flight spectra returns.

In lieu of the closed loop tests, the open loop performance of the automatic slope controller was tested utilizing fixed error signals as inputs. These tests were very satisfactory and, therefore, it is not felt that sufficient additional data would be gathered by performing closed loop tests to justify the design and construction of another bandwidth simulator.

Voltage Waveform Generator

No changes to the design of this unit have been made since the last report. Provisions were made to generate both positive and negative parabolic waveforms for the manual flight test unit. A negative parabolic waveform has been shown to be of no value and will not be included in the new waveform generator (located in the computer and control unit). The high frequency triodes used in the operational amplifiers have displayed a susceptibility to acoustic noise at a natural resonant frequency of 7 to 8 kc. Use of acoustic shielding has reduced the noise to acceptable levels. In all other respects the waveform generator has been extremely reliable.

2.1.2.2 Doppler Frequency Computer

A flyable breadboard of the Doppler Frequency Computer has been fabricated and is nearing completion of laboratory testing. A block diagram of the computer is shown in Figure 2-16. To measure the computer's performance, both inputs (points A and K in Figure 2-16) were fed from the same signal source. The equation to be solved was derived in Section 2.1.2 as Equation (2-22). This may be rewritten as:

$$\frac{f_{D_i}}{K} = 2(0.81250)f'_{B_i} - 2f''_{B_i} \qquad (2\text{-}24)$$

where

$$K = \frac{2}{5.333}$$

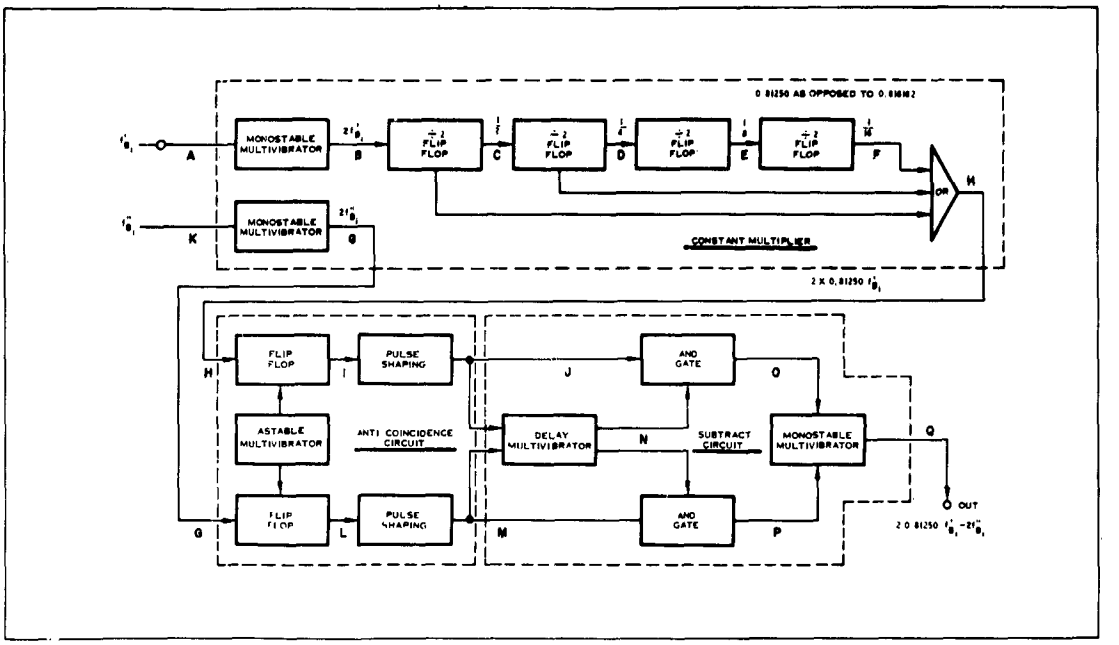

Figure 2-16 - Doppler Frequency Computer, Block Diagram

For the laboratory test, both f'_{B_i} and f''_{B_i} were set equal to 25, 032. 9 cps. Substitution of this value into Equation (2-24) yields:

$$\frac{f_{D_i}}{K} = 9387 \text{ cps} \qquad (2\text{-}25)$$

and this represents the desired computer output. Table 2-1 lists the frequencies registered at the various test points, and shows the computer output (point Q) to be at the desired frequency. In Figure 2-16, point H is the summation of the pulse rates from points C, D, and F.

A further observation may now be made. The application of a 21, 666 cps square signal to points A and K of Figure 2-16 will result in an output pulse train frequency of 8125 cps, which is in precise numerical agreement with the multiplication factor of 0. 81250, appearing in Equation (2-24). This test is proposed as a simple in-flight technique for computer checkout.

TABLE 2-1

NUMERICAL RESULTS OF DOPPLER FREQUENCY COMPUTER TEST

Signal Flow Points	Frequency (cps)
A	25032.9
B	50064.5
C	25032.2
D	12516.0
E	6257.9
F	3129.0
G	50065.8
H	40676.0
I	40675.0
J	40675.0
K	25032.9
L	50063.9
M	50063.0
N	40675.0
O	---
P	---
Q	9387.0

2.2 Flight Test Results

In Section 4 of both References 5 and 6, the flight test plan and objectives were discussed. The objectives are listed here again for expediency. They are:

1) to show that the application of FM to the transmitter can simultaneously increase the peak power spectral density while decreasing the absolute signal bandwidth;
2) to show that a reduction in signal bandwidth also produces a reduction in the fluctuation and terrain bias errors;
3) to experimentally compare the accuracy of a spectral compression system with a single channel CW system.

In addition to these general objectives, other effects were to be investigated; namely,

4) the effect of drift angle on spectral compression;
5) the effect of different types of terrain (water and smooth and rough land);
6) the effect of different peak transmitter deviations;
7) the effectiveness of the second order modulation (parabolic);
8) pitch and roll fluctuation effects;
9) the operation of the automatic slope control loop; specifically, accuracy vs speed of response.

During this first flight test period, the major effort was directed toward objective 1). Some system improvements were added, flight test procedures altered to achieve best results, and data recording techniques improved in order to preserve the results observed in real time during the flight test.

Though the exact speeds, altitudes, and geographic areas varied during the flight tests, the general flight test plan remained the same except for the last flight. Regardless of speed or altitude, the heading of the B-26 Flight Test Aircraft (Figure 2-17) was established at a near zero drift angle condition. The flights were planned so that half of the run was over relatively flat land, and the other half over water (off Boston harbor). After ten to fifteen minutes over water, the aircraft heading was reversed and the same ground path followed on the inbound heading. About ten minutes of land data per run were recorded before the next heading reversal.

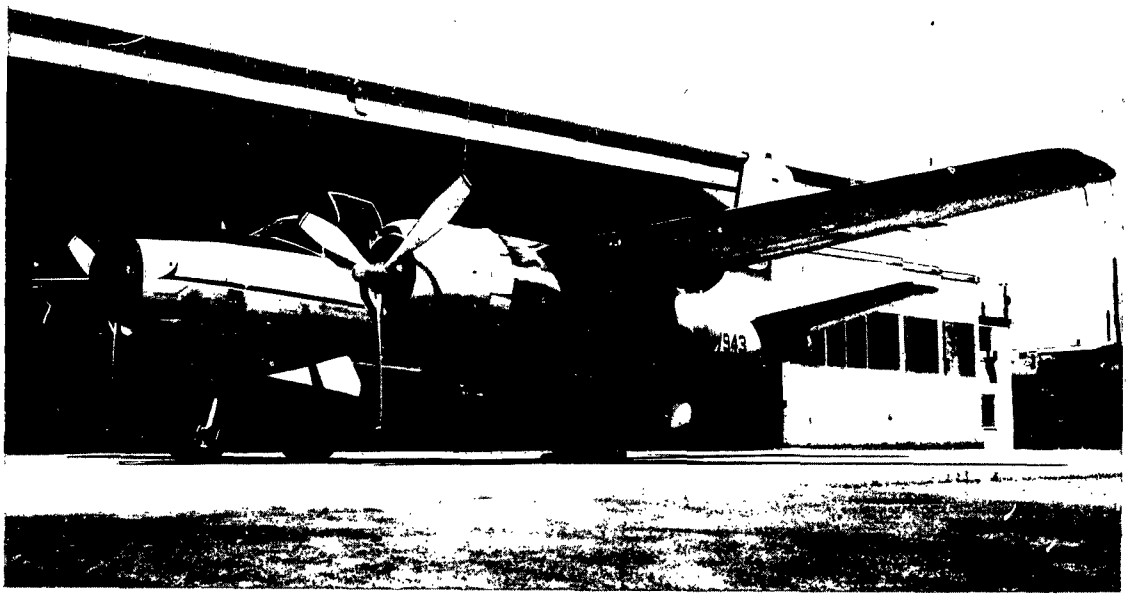

Figure 2-17 - Flight Test Aircraft (B-26)

A typical flight run would be performed as follows:

1) Check for near zero drift angle condition and note type of terrain. Change aircraft heading as necessary to meet zero drift angle condition.
2) With tape recorder operating and with the transmitter in CW mode, measure the doppler frequency by using a marker oscillator.
3) Using Figure 2-18, determine the ground speed. (For example, a doppler frequency of 3 kc would indicate a ground speed of 190 kts. From the ground speed of 190 kts, the optimum beat frequency of 19.7 kc may be determined.)
4) The correct linear modulation slope may be determined by proceeding vertically from 190 kts to an altitude line, say 8000 ft, and then moving horizontally to the left to a linear slope (M_1) setting of 2.68. This value would then be established by adjustment of the linear slope control at a PRF of 20 cps.

5) While observing the spectrum analyzer in the region of 20 kc, the linear slope would be changed about the value of 2.68, as required, to achieve best compression.

6) Next, the PRF would be lowered to 10-15 cps. The correct value of parabolic would be determined using Figure 2-19 by again proceeding vertically from the 190 kts ground speed line to the 8000 ft altitude line and then horizontally to the left to an M_2 setting of 5.12. Again, as in the case of the linear slope, the parabolic control would be adjusted for best compression. Providing best linear slope has been established, there should be no need to readjust the linear slope after adding the parabolic correction.

During all flights, the raw video receiver data was tape recorded and at least the following items were voice recorded:

Altitude	Type of Terrain
True Air Speed	PRF
Linear and Parabolic Slope Settings	Power Output

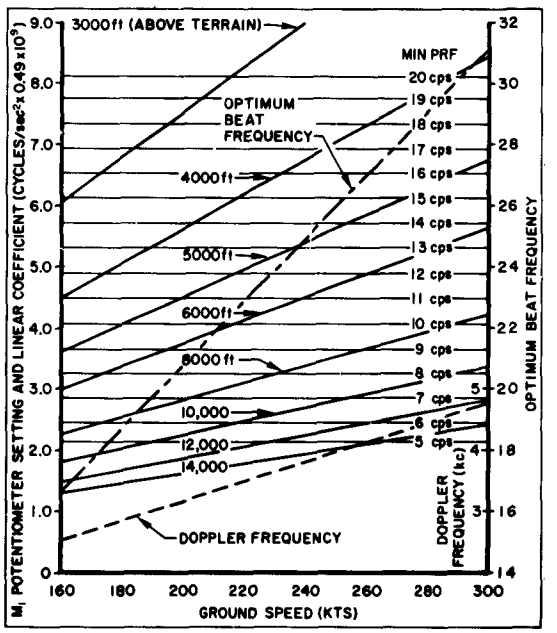

Figure 2-18 - In-Flight Test Parameters, Linear Modulation

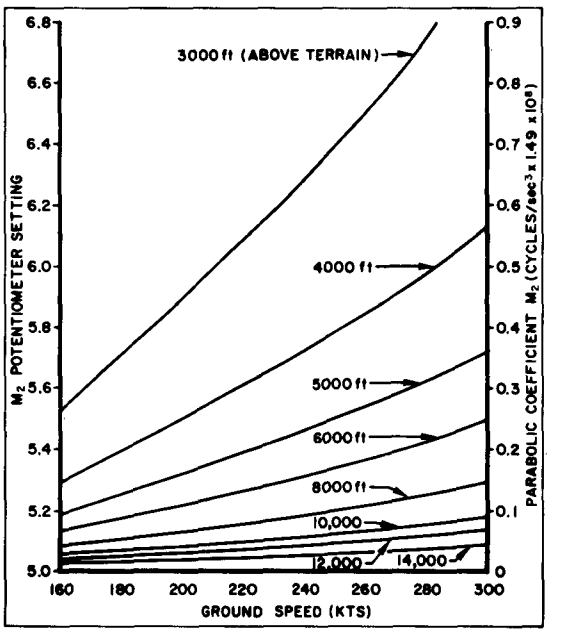

Figure 2-19 - In-Flight Test Parameters, Parabolic Modulation

Motion pictures of the spectrum analyzer output were taken for backup information.

The following is a brief summary of the spectral compression flights, to date, covering the difficulties overcome and the performance achieved.

Flight No. 1 -- 1 April 1963

Conditions	Performance
a) 2, 500 feet, over water, CW transmission.	The effect of excess FM noise (due to acoustic noise) was evident. Increased engine power in climbs completely smears the spectrum.
b) 4, 000 ft, CW.	FM noise effects more pronounced.
c) 3, 000 ft, CW, 176 kts ground speed, flight over runway at Hanscom Field, heavy air turbulence.	Reference run to test modulation.
d) 3, 000 ft, linear modulation, 176 kts ground speed over runway, nonoptimum modulation slope.	Compression of 2 - 3:1 achieved.

Flight No. 2 -- 3 April 1963

Conditions	Performance
1, 500 feet over land.	Unable to close VCO loop.

Flight No. 3 -- 9 April 1963

Conditions	Performance
3, 000-6, 000 feet over land and water.	Still experienced FM noise difficulties after rework of VCO loop.

Flight No. 4 -- 26 April 1963

Conditions	Performance
a) 3, 000 ft over land and slight sea. Acoustic shielding of nuvistors added to operational amplifiers.	Much improved CW performance. Some evidence of specular FM noise present, but considerably reduced over previous flights. Compression ratios of 3-5:1 achieved.
b) 4, 000 and 5, 000 feet over land and slight sea.	Much improved CW and linear modulation performance.

Flight No. 5 -- 9 May 1963

Conditions	Performance
3,000-4,000 feet over land and calm sea.	Same performance as Flight No. 4. Unable to get above 4,000 feet because of clouds, and unable to get sea return because of low winds.

Flight No. 6 -- 13 May 1963

Conditions	Performance
4,000-8,000 feet over land and water.	Good CW performance at 8,000 feet. Tape recorder failure. Compression still 3-5:1.

Flight No. 7 -- 17 May 1963

Conditions	Performance
8,000 feet over land and water. Spectral compression flight charts (Figures 2-18 and 2-19) updated.	Improved compression performance.

Flight No. 8 -- 24 May 1963

Conditions	Performance
8,000 feet over land and water. Parabolic correction used. Motion picture recording and doppler mixer used to reduce tape flutter and wow before recording. PRF of 10-15 cps.	Very good compression, 9-10:1. Parabolic correction very effective at PRF of 10 cps. Rough terrain effects decrease compression ratio over land, as was expected.

Flight No. 9 -- 27 May 1963

Conditions	Performance
8,000-9,000 feet over land, 200-220 kts ground speed.	Cross country flight to ASD. Change in degree of compression observed in passing from flat to rough terrain. Compression performance as good as Flight No. 8 over flat land.

Because this series of flight tests was not quite complete at the close of this reporting period, a complete data analysis could not be presented in this report. However, Figures 2-20 and 2-21 show a comparison of CW data with one of the better spectral compression runs. Figure 2-20 shows CW return at 8,000 feet over water, a ground speed of 210 kts, a doppler frequency of 3350 cps, and a doppler bandwidth of 360 cps ($\approx$ 10.7% bandwidth). The analyzer

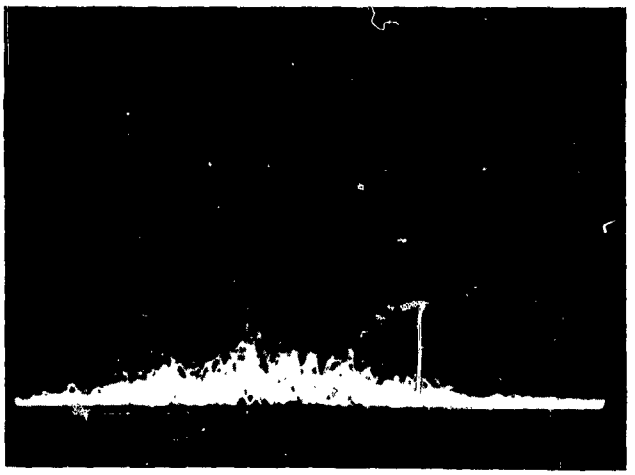

Figure 2-20 - CW Spectrum

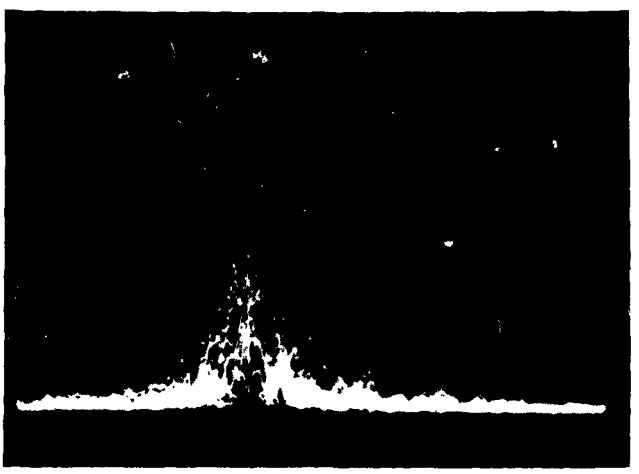

Figure 2-21 - Compressed Spectrum

sweep rate is 100 cps per cm, and the peak spectral density amplitude is about 1.2 cm high. Figure 2-21 shows a compressed spectrum at the same flight conditions as Figure 2-20. The beat frequency appears at 20.8 kc, the PRF is 15 cps, the linear slope set at 2.6, and the parabolic at 5.8 - 6.4. The compressed bandwidth is 40 cps (a 9 to 1 reduction), and the peak spectral density amplitude is about 4.2 cm high. This analyzer presentation is voltage vs frequency and, therefore, one would expect about a three to one increase in peak spectral density (9 to 1 in power). The compressed spectrum data of Figure 2-21 is in fact pessimistic in that this data was taken before the decision was made to heterodyne the beat frequency to 2 kc before recording. As a result, the degrading effects of tape flutter and wow are still present. As the compression bandwidths approached 30-60 cps (as compared with a CW bandwidth of 300 to 350 cps), the effects of tape recorder flutter and wow became evident.

2.2.1 Tape Flutter

Measurements made on the tape recorder used in the flight tests indicated that data smearing occurred that was proportional to the frequency being recorded. At 17 kc, smearing amounted to about 40 cps while at 30 kc, as much as 130 cps of smearing was measured. Since most of the data from the B-26 flight tests occur in the range of 15 kc to 30 kc, one decided that some improvement in data recording would be needed. What has been done is to heterodyne the doppler signal with a variable oscillator to produce an output in the frequency range of 2 kc to 3 kc. In this recording range, tape flutter is greatly reduced (to about 5 cps). The schematic diagram of the mixer circuit is shown in Figure 2-22.

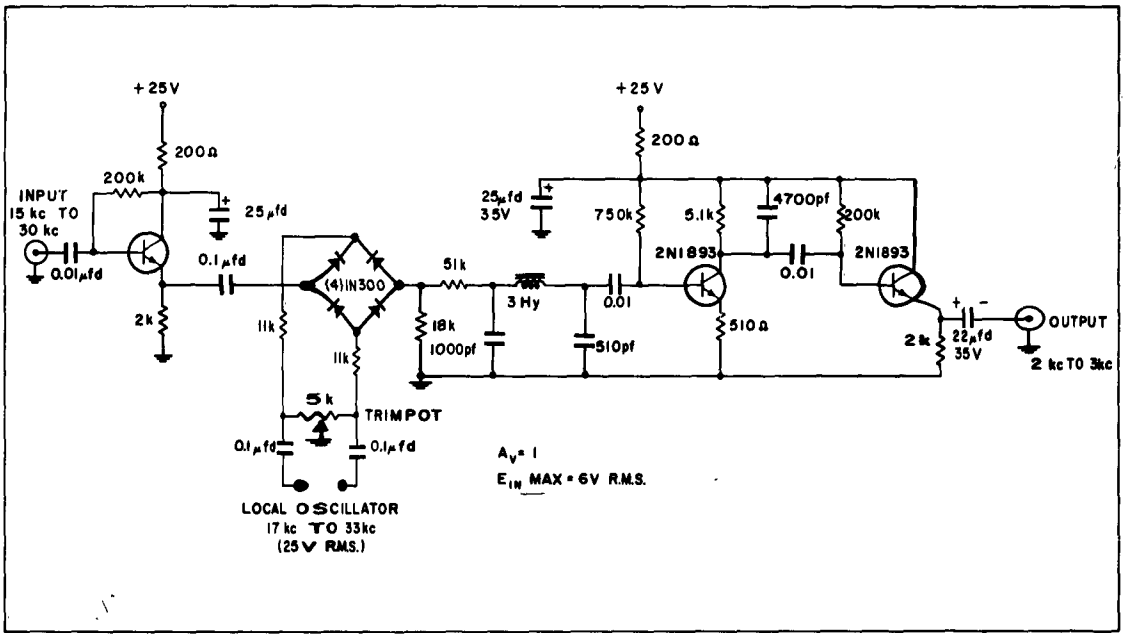

Figure 2-22 - Doppler Mixer, Schematic

2.3 Theoretical Aspects of Spectral Compression

2.3.1 Optimum Filtering and Optimum Bandwidth Sensor Studies

The problem of estimating the bandwidth of a band of Gaussian noise in a background of other noise (e.g., white noise), can be treated by means employed in the first ADVS program (Reference 2). This analysis indicates that a suitable filtering of the power spectrum of the ground echo is the proper type of processing, and indicates what type of filter to use. An even more convenient form of discussion is obtained if one uses the information gained by decision theory that a suitable filter is optimum, and then looks for such a filter. The decision theory is sufficiently specialized that one relegates it to Appendix A. The filtering analysis is presented in the next section.

2.3.1.1 Optimum Filtering for Bandwidth Sensing

The bandwidth estimate, $\hat{B}$, is derived from the power spectrum of signal and noise, P (f, B). In the power spectrum, the dependence on the actual bandwidth is indicated explicitly. To this spectrum, one applies a filter whose power response vs frequency is indicated by D (f). One envisages a closed loop form of sensing, and therefore subtracts from the output the value for the proper bandwidth. This is a constant and, therefore, can be determined in advance; i.e., the amount subtracted to provide an error signal can be considered to be the value for the proper bandwidth, since the deviation of the closed loop output from the proper value is very small. The estimate is thus,

$$\hat{\delta B} = K\left[\int D(f)\,\hat{P}(f, B)\,df - \int D(f)\,P(f, B)\,df\right] \qquad (2\text{-}26)$$

The estimate is then actually of the error signal; i.e., of the amount that the current estimate should be changed to equal the proper value and, therefore, is indicated as an estimate of a small quantity. If one provides an unbiased estimate of the spectrum, $\hat{P}$, the error signal estimator is itself unbiased; i.e., on the average, it gives the true error signal although, of course, exhibiting random fluctuations.

The filter is required to provide an adequate error signal before minimizing fluctuation. Therefore, one requires as a side condition that those filters which are compared (to find the optimum) shall all provide the same error signal. This condition can be incorporated directly into the denominator of the expression for the estimator. Since one deals with closed loop estimators, only small error signals are to be expected, so that a Taylor expansion will determine the error signal, namely:

$$\langle \hat{\delta B} \rangle = K \left[\int D(f) \left\{ P(f, B) + \delta B \frac{\partial}{\partial B} P(f, B) \right\} df \right.$$

$$\left. - \int D(f) P(f, B)\, df \right] \tag{2-27}$$

$$= K \delta B \int D(f) \frac{\partial}{\partial B} P(f, B)\, df \tag{2-28}$$

The final form for the estimator is then:

$$\hat{\delta B} = \frac{\int D(f) \left[\hat{P}(f, B) - P(f, B) \right] df}{\int D(f) \frac{\partial}{\partial B} P(f, B)\, df} \tag{2-29}$$

The fluctuations in the estimate depend on fluctuations in the estimate of the spectrum. These have been thoroughly discussed before in the first ADVS program (References 3 and 4) and, therefore, one can apply the results here immediately. In the first place, spectrum estimates derived by the methods of Blackman and Tukey, for instance, are unbiased, and the variance of the spectral estimates, under conditions satisfied in navigator applications, is given by:

$$\langle \hat{P}(f, B) \hat{P}(g, B) \rangle - \langle \hat{P}(f, B) \rangle \langle \hat{P}(g, B) \rangle = \frac{\delta (f-g)}{T} P(f, B) P(g, B) \tag{2-30}$$

where $\delta (f-g)$ is the delta function and T is the averaging time.

The variance of the error signal estimate is then:

$$E^2 = \frac{\int D^2(f)\, P^2(f, B)\, df}{T\left[\int D(f) \frac{\partial P}{\partial B}\, df\right]^2} \tag{2-31}$$

Now the spectrum is given by the sum of a noise plus a signal part which alone contains the bandwidth which one seeks to determine:

$$P(f, B) = S\, w\left(\frac{f}{B}\right) + N \tag{2-32}$$

Here the noise is taken as white, with a spectral level of N watts/-cps. Other shapes of noise can be just as easily handled. Note that the noise spectrum is assumed known. This is ordinarily valid since the noise level is associated with the receiver, rather than the transmission path. The peak signal spectrum level is S and the normalized shape of the signal spectrum is then w. The bandwidth enters as a scaling factor of the frequency dependence. The derivative required is then:

$$\frac{\partial P(f, B)}{\partial B} = -\frac{S}{B^2} f\, w'\left(\frac{f}{B}\right) = -S \frac{f}{B} \frac{\partial}{\partial f} w\left(\frac{f}{B}\right) \tag{2-33}$$

where w' indicates the derivative of the spectrum with respect to $\frac{f}{B}$.

The Euler-Lagrange equation is then:

$$\frac{\partial}{\partial D}\left[D^2_{opt} P^2 - \lambda D \frac{\partial P}{\partial B}\right] = 0 \tag{2-34}$$

which yields

$$2 D_{opt} P^2 = \lambda \frac{\partial P}{\partial B} \tag{2-35}$$

and

$$D_{opt} = (\text{const.}) \frac{f \frac{\partial}{\partial f} w}{(S w + N)^2} \tag{2-36}$$

In the white noise case, where the noise spectrum is independent of frequency, the optimal filter characteristic can be written as:

$$D_{opt} = (\text{const.})\,(f)\,\frac{\frac{\partial}{\partial f} P\,(f)}{P^2\,(f)} \tag{2-37}$$

This is similar, but not identical, to the filter which is optimal for sensing velocity, found in Reference 3. The bandwidth filter differs in having an additional f weighting, i. e., a rising 3 db/octave slope in addition to the characteristic of the velocity filter.

2. 3. 1. 2 Discussion of the Optimum Filter

The presence of the extra f weighting in the bandwidth filter, as compared to the velocity filter, is an advantage in that the optimal filter is realizable exactly as a lumped constant network if the signal spectrum is also realizable. In point of fact, the signal spectrum is due primarily to the transmitting and receiving antenna patterns and, thus, is not exactly realizable as a lumped constant network. However, if a realizable approximant to the spectrum can be devised, a realizable filter optimum for the approximant can be found. This is not possible in the velocity filter case, where it is necessary to approximate a $\sqrt{f}$ characteristic (in voltage response). For instance, if one again uses a Butterworth signal spectrum as an example:

$$w\,(f/B) = \frac{1}{1 + (f/B)^{2p}} \tag{2-38}$$

and

$$D_{opt} = (\text{const.})\,(f)\left(\frac{2p\,(f/B)^{(2p-1)}}{\left[1 + (f/B)^{2p}\right]^2}\right)\left(\frac{S}{1 + (f/B)^{2p}} + N\right)^{-2} \tag{2-39}$$

Eliminating common factors, and changing the value of the constant, one obtains the form:

$$D_{opt}(f) = (\text{const.})\left(\frac{f^{2p}}{\left[B^{2p}\left(1+\frac{S}{N}\right)+f^{2p}\right]^2}\right) \qquad (2\text{-}40)$$

This corresponds to a cutoff at the same rate as for the signal spectrum, with a corner frequency somewhat above the signal spectrum carrier frequency and a rising characteristic at the same rate with the same corner frequency.

The optimum filter depends on both the signal-to-noise ratio and signal bandwidth. The dependence of both the filter characteristic and its performance are not sensitive to the signal-to-noise ratio, so that a design fixed in this respect can expect to provide satisfactory performance. On the other hand, the performance is sensitive with respect to bandwidth.

The results of the investigation of optimal velocity filters, mismatched with respect to bandwidth, although not yet complete, indicate that drastic degradation in performance can be expected if spectra substantially narrower than the value for which the filter was designed are used. This effect seems to be principally due to the hole in the optimum filter response at the center.

Thus, it would appear that if a fixed design is to be employed for a range of spectral widths, the rising characteristic should not be so steep as would be indicated by the optimal filter for a fixed width. Quantitative evaluation of the relationship is not available at this time.

A nutating bandwidth sensor should be designed with optimum filtering of the type derived above for each nutation channel. The nutation principle does not affect the fluctuation performance, since the duration of each half of the nutation switching must be long enough to obtain an error sense, which implies an averaging time long enough to give independence of the fluctuations on adjacent portions of the nutation cycle.

2.3.1.3 Conclusions

1) The optimal closed loop bandwidth sensor has the form of a filtering of the power spectrum of the radar echo. This type of processing can be implemented in many ways. If the effective loop gains are made equal, the relative performance depends only on the filtering.

2) The power response of the optimal filter, with a background of white noise, is f $P'(f)/P^2(f)$, where $P(f)$ is the power spectrum of signal and noise and $P'(f)$ is the derivative of the spectrum with respect to frequency.
3) If a fixed design is to be employed for a range of spectra of differing widths, the filter characteristic should be somewhat less sharply rising and falling than indicated by the prescription which is optimum at a fixed bandwidth.

3. CONCLUSIONS

The first series of manual spectral compression flights was completed. Spectral analysis shows a 9:1 compression ratio, along with the corresponding 3:1 increase in peak voltage spectral density (as compared to the CW return). This degree of compression was obtained by using a large coefficient of linear frequency modulation and a small degree of second order correction. A more complete analysis of the flight test data is expected to yield more information on the spectral compression phenomena, such as: sensitivity; bias error reduction; peak deviation effects; etc.

Measurements made on the diode-rate-counter used to linearize the VCO indicate that a linearity of 0.012% has been achieved.

Installation of the second microwave multiplier achieved the required transmitter performance in terms of passband AM. Less than 0.5 db of variation exists over the range of 200 mc.

The acoustic noise sensitivity of the equipment was remedied by the addition of acoustic shielding and tube selection. Flights as high as 10,000 feet were conducted following the acoustic noise reduction effort. In developing a transmitter for operation at orbital altitudes, special care in transmitter design, components selection, and fabrication would be required.

A complete, flyable model of the Computer and Control Unit was fabricated and is now undergoing laboratory checkout. Special attention was paid to the bandwidth sensor, which is a vital part of the automatic slope control loop. A theoretical study defined the optimum filtering characteristic for the bandwidth sensor. Specifically, the study concluded that the rise and fall characteristic should match the spectrum rise and fall. Actual bandwidth sensor measurements, with and without the optimum filtering networks, showed that the use of the optimum networks improved the band-with sensor scale factor and reduced the output fluctuations. With or without the networks, the output of the sensor still increases directly with bandwith over the range of interest.

4. PROGRAM FOR THE NEXT INTERVAL

In general, the effort for the next period will be directed toward meeting the objectives and investigating the effects presented in Section 2.2, Flight Test Results.

Specifically, the ground checkout of the flyable Computer and Control unit will be completed, the spectral compression system will be reinstalled in the B-26 aircraft with the new Computer and Control unit, data recording procedures and instrumentation will be modified for the second series of flight tests, the second series of spectral compression flights will be performed, and the data analyzed and compared to predicted performance. In addition, the data from the first series of flight tests will be more thoroughly analyzed, and a more detailed coverage of the flights presented in the final program report.

APPENDIX A
DECISION THEORY FORMULATION FOR BANDWIDTH SENSING

The analysis of the corresponding problem for velocity sensing has been carried out in the first ADVS program (Reference 2, Appendix A). The early part is concerned with the problem in the general form of estimating a parameter of the noise band which represents the signal in the presence of background noise. At this level of generality, the previous analysis applies directly, so that here one needs only sketch the initial stages of the derivation.

The estimate, γ^*, of the parameter θ, which here represents bandwidth, is given by the average of θ over the probability distribution of θ conditioned on the received waveform:

$$\gamma^* (\overline{V}) = \int \theta \, w (\theta / \overline{V}) \, d\theta \qquad (A-1)$$

where the vector $\overline{V}$ is a full collection of samples of the waveform of signal plus noise.

By transformations described in detail in Equation (A-18) of Reference 2, the estimator can be expressed as:

$$\gamma^* (\overline{V}) = \langle\theta\rangle - a^{-2} \left[\left\langle \overline{V}^T (\theta - \langle\theta\rangle) \overline{\overline{k}}_S^{-1} \overline{V} \right\rangle - \left\langle (\theta - \langle\theta\rangle) \, t_r \, \overline{\overline{k}}_N \overline{\overline{k}}_S^{-1} \right\rangle \right] \qquad (A-2)$$

where higher order terms have been eliminated as insignificant.

Here a^2 is the signal-to-noise power ratio at the input to the bandwidth sensor, where it is moderately large; $\overline{\overline{k}}_N$ and $\overline{\overline{k}}_S$ are the normalized covariances of noise and signal, respectively; t_r stands for the trace operation; and the averages (indicated by pointed brackets) are over the unconditional distribution of θ.

With a closed loop sensor, the error signal, $\hat{\delta\theta}$, is derived from the second term alone, since neither the first (a priori) term nor the last (bias) term depend on the waveform received. Thus:

$$\hat{\delta\theta} = -a^{-2} \left\langle (\theta - \langle\theta\rangle) \, \overline{V}^T \overline{\overline{k}}_S^{-1} \overline{V} \right\rangle \qquad (A-3)$$

The a priori distribution of θ is effectively Gaussian about its true value because of the centering action of the closed loop. The second term can then be integrated by parts with respect to θ, to yield:

$$\hat{\delta\theta} = \frac{\sigma^2}{a^2} \int \overline{V}^T \overline{\overline{k}}_S^{-1} \overline{V} \frac{\partial}{\partial\theta} \exp. \left[\frac{(\theta - \langle\theta\rangle)^2}{2\sigma^2} \right] \frac{d\theta}{\sqrt{2\pi\sigma^2}} \tag{A-4}$$

$$= -\frac{\sigma^2}{a^2} \frac{\partial}{\partial\theta} \overline{V}^T \overline{\overline{k}}_S^{-1} \overline{V} \Big|_{\langle\theta\rangle} \tag{A-5}$$

The integration over θ can be carried out assuming the quadratic form constant at the mean value of θ, because of the closed loop.

With continuous sampling over a long time interval, the quadratic form goes over to a double integral:

$$\hat{\delta\theta} = -\frac{\sigma^2}{a^2} \frac{\partial}{\partial\theta} \iint V(t)\, k_S^{-1}(t - \tau)\, V(\tau)\, dt\, d\tau \Big|_{\langle\theta\rangle} \tag{A-6}$$

By transforming from this time domain form to the frequency domain, one gets:

$$\hat{\delta\theta} = -\frac{\sigma^2}{a^2} \frac{\partial}{\partial\theta} \int |v(f)|^2 w_S^{-1}(f)\, df \tag{A-7}$$

This represents a substantial simplification, because the convolution theorem allows the reduction of the right hand side from a double integral to a single one. The quantity $|v(f)|^2$ is, then, the estimate of the power spectrum of the input. The weighting factor $w_S^{-1}(f)$ (where $w_S^{-1}(f)$ is the Fourier transform of $k_S^{-1}(t)$) is also much simpler than the time domain weighting factor. In the time domain $k_S^{-1}(t)$ is the operator inverse to the signal covariance, i.e.:

$$\int k_S(t - \tau)\, k_S^{-1}(\tau)\, d\tau = \delta(t) \tag{A-8}$$

so that the minus one is symbolic of this inverse relationship. The frequency domain form of this equation is, however:

$$w_S(f)\, w_S^{-1}(f) = 1 \tag{A-9}$$

that is, the minus one can now be considered merely as an exponent. In the language of functional analysis, one would say that the covariance becomes diagonal in the frequency domain representation, so that the spectrum of the inverse in this representation is given by the reciprocal of the eigenvalue spectrum of the covariance.

Now finally, one can specialize the problem to a search for bandwidth. The bandwidth appears in the power spectrum as a scaling factor:

$$\hat{\delta\theta} = -\frac{\sigma^2}{a^2}\int |v(f)|^2 \frac{\partial}{\partial\theta}\frac{1}{w_S(\frac{f}{\theta})}\,df \qquad \text{(A-10)}$$

$$= \frac{\sigma^2}{a^2}\int |v(f)|^2 \frac{f}{\theta}\frac{\frac{\partial}{\partial f}w_S(\frac{f}{\theta})}{w_S^2(\frac{f}{\theta})}\,df \qquad \text{(A-11)}$$

This last equation states that the optimum estimator has the form of a filtering of the estimated power spectrum. The characteristic of the filter is the same as that found from the filtering analysis of Section 2.3 in the main body of this report (to within terms of higher order in a^{-2}).

Thus, the decision theory and filtering theory analyses are in mutual agreement. The decision theory derivation is, in principle, more general. However, in order to find an explicit form for the estimator, one was required to limit oneself to the strong signal case, which in fact, is the only important one. The filtering theory result is valid for all values of signal-to-noise ratio, but assumes a priori that filtering the spectral estimate is the proper thing to do. In the region of practical importance, where both theories apply, their predictions are mutually concordant.

APPENDIX B
BIBLIOGRAPHY

(1) "Investigation of Active Doppler Velocity Sensor", Quarterly Engineering Report No. 3 on Contract AF33(657)-9241, Raytheon Report No. BR-2311, dated March 1963.

(2) "Investigation of Active Doppler Velocity Sensor", Quarterly Engineering Report No. 3 on Contract AF33(616)-7388, Raytheon Report No. AED-430, Section 2.4.1 and Appendix A, dated March 1961.

(3) "Investigation of Active Doppler Velocity Sensor", Quarterly Engineering Report No. 2 on Contract AF33(616)-7388, Raytheon Report No. AED-407, dated December 1960.

(4) Mullen, Dr. J.A., "Optimal Filtering for Radar Doppler Navigators", IRE International Conventional Records, 1962, Part 5, pp. 40-48.

(5) "Investigation of Active Doppler Velocity Sensor", Quarterly Engineering Report No. 1 on Contract AF33(657)-9241, Raytheon Report No. BR-1975, dated September 1962.

(6) "Investigation of Active Doppler Velocity Sensor", Quarterly Engineering Report No. 2 on Contract AF33(657)-9241, Raytheon Report No. BR-2144, dated December 1962.

RAYTHEON

DISTRIBUTION LIST

Distribution List for Raytheon's Quarterly Engineering Reports under Contract AF 33(657)-9241.

Qty.	
1	Headquarters Aeronautical Systems Division Attn: ASNR Wright-Patterson Air Force Base Ohio
1	Headquarters Aeronautical Systems Division Attn: ASAPR Wright-Patterson Air Force Base Ohio
1	Director Research and Development Headquarters U. S. Air Force Attn: AFDRD-CC Washington 25, D. C.
3	Headquarters Aeronautical Systems Division Attn: ASRNGE-2, Mr. Guidice Wright-Patterson Air Force Base Ohio
8	Headquarters Armed Services Technical Information Agency Attn: TIPDR Arlington Hall Station Arlington 12, Virginia
1	The Rand Corporation Engineering Division 1700 Main Street Santa Monica, California Attn: Mr. R. W. Buchheim
1	Headquarters Space Systems Division Air Force Unit Post Office Attn: Capt. H. O. Hall Los Angeles 45, California

Qty.	
1	Headquarters Air Force Cambridge Research Laboratory Electronic Research Directorate Attn: CRRDM, Mr. Walter Rotman L. G. Hanscom Field Bedford, Massachusetts
1	Headquarters Aeronautical Systems Division Attn: ASNV Wright-Patterson Air Force Base Ohio
1	Jet Propulsion Laboratory 4800 Oak Grove Avenue Pasadena, California Attn: Mr. Henry A. Curtis
1	Hughes Aircraft Company Aerospace Engineering Division Culver City, California Attn: Dr. W. Kummer
1	National Aeronautics and Space Administration Space Task Group Langley Field, Virginia
1	National Aeronautics and Space Administration Lewis Research Center 21000 Brookpark Road Cleveland 35, Ohio Attn: Library, Mr. G. Mandel
1	Headquarters Aeronautical Systems Division Attn: ASRSMX-10 Wright-Patterson Air Force Base Ohio
1	Headquarters Aeronautical Systems Division Attn: ASNRT Wright-Patterson Air Force Base Ohio
1	Headquarter Aeronautical Systems Division Attn: ASNSEB-2 Wright-Patterson Air Force Base Ohio